

Supplementary Information

Non-Oxidative, Controlled Exfoliation of Graphite in Aqueous Medium

Pawan Kumar Srivastava, Premlata Yadav and Subhasis Ghosh*

*E-mail: Subhasis@jnu.ac.in

School of Physical Sciences, Jawaharlal Nehru University, New Delhi-110067

Contents

S1.0 Schematic of exfoliation mechanism

S2.0 Dispersion of graphene flakes

S3.0 Correlation of AFM height profiles and Raman spectroscopic signatures

S4.0 Graphene in water: Stability in a non-stabilizing medium

S5.0 AFM imaging of aged samples

S6.0 Dynamic light scattering experiment: Flake size determination of suspended graphene layers in Dispersion

S7.0 Recycling of the sediment

S8.0 AFM topographic images for graphene layers obtained by exfoliation of LDG in water

S9.0 Scanning electron micrograph of graphene samples prepared from exfoliation of LDG in Water

S10.0 TEM image of graphene exfoliated in water (using LDG)

S11.0 TEM image of graphene exfoliated in heavy water

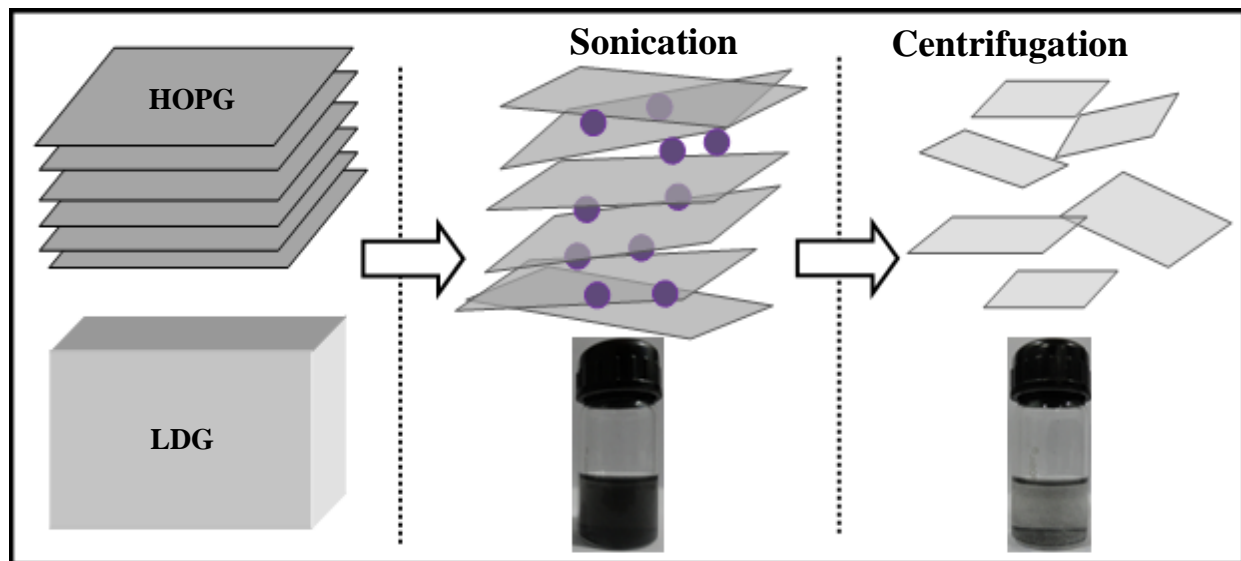
S12.0 Lorentzian fitting of 2D peak of graphene: Identification of layered structure

S13.0 Confocal Raman mapping and spectroscopy for graphene exfoliated in water

S14.0 Electronic structure calculations

S14.1 Simulated infrared spectra

S1.0 Schematic of exfoliation mechanism



● —————> Solvent molecules

Figure S1. Schematics of liquid phase exfoliation of HOPG/LDG into thin graphene layers which involves sonication of HOPG or LDG in desired solvents and then the sonicated dispersion is centrifuged to isolate thin graphene layers from bulk graphitic flakes. During sonication, solvent molecules act as intercalates for breaking the van der Waals interaction between graphitic layers in HOPG/LDG, and finally thin graphene layers can be obtained. Centrifugation of the sonicated dispersion results in the precipitation of thick graphitic flakes. Snapshots of sonicated and centrifuged solutions are also given.

S2.0 Dispersion of graphene flakes:

The layered structure of graphene can be characterized by various spectroscopic and imaging techniques such as Raman spectroscopy¹, HRTEM², electron diffraction and atomic force microscopy³. In this work, more than 200 graphene flakes were first identified by inspection under optical microscope and later thickness and morphology were monitored using atomic force microscopy (Figure S6, S7 and table S1) to quantify the number fractions, mass fractions and overall yield of graphene layers obtained from water/HOPG based dispersions. We generated a statistics of no. of times of different no of layers obtained, based on the visual observations, as shown in Figure S5. In this case the number fraction of graphene monolayers for fresh dispersion is around 40%. We have also calculated the mass fraction of graphene which is defined as⁴

$$\frac{M_{mono}}{M_{all}} = \frac{\sum_{individual} A_{mono}}{\sum_{all} N_{mono} A_{mono}} \quad (1)$$

Where A_{mono} is the area of monolayer and N_{mono} represents the number of monolayers in a given flake. The mass fraction for graphene monolayers obtained using fresh water/HOPG dispersion was found to be ~16.6 wt%. Mass fraction of graphene monolayers can be used to calculate the overall yield using relation⁴

$$Y = \left(\frac{M_{mono}}{M_{all}} \right) \times \delta \quad (2)$$

Where, δ is the remaining fraction of sediment after centrifugation. So, the dispersion ability (yield) of graphene flakes can be characterized by the fraction of graphene or thick graphitic flakes remaining after centrifugation. Figure S2.a shows optical absorbance plotted against wavelength

for different concentrations of water/HOPG dispersions. Concentration of dispersion was varied by repeated dilution. Optical absorbance (at $\lambda=660$ nm) divided by cell length is plotted versus concentration which shows Beer-Lambert behavior with molar absorptivity (α_{660}) of $1200 \text{ L-gm}^{-1} \text{m}^{-1}$ (Figure S2.b). Molar absorptivity and optical absorbance are related through the equation-

$$\frac{A}{l} = \alpha \times C. \quad (3)$$

where, A is optical absorbance; l , cell length; α , molar absorptivity and C , concentration of the dispersion. Remaining fraction after centrifugation (δ) was calculated using measured absorption coefficient after centrifugation and average molar absorptivity (α_{660}) $\sim 1200 \text{ L-gm}^{-1} \text{m}^{-1}$ (Fig. S2.b).

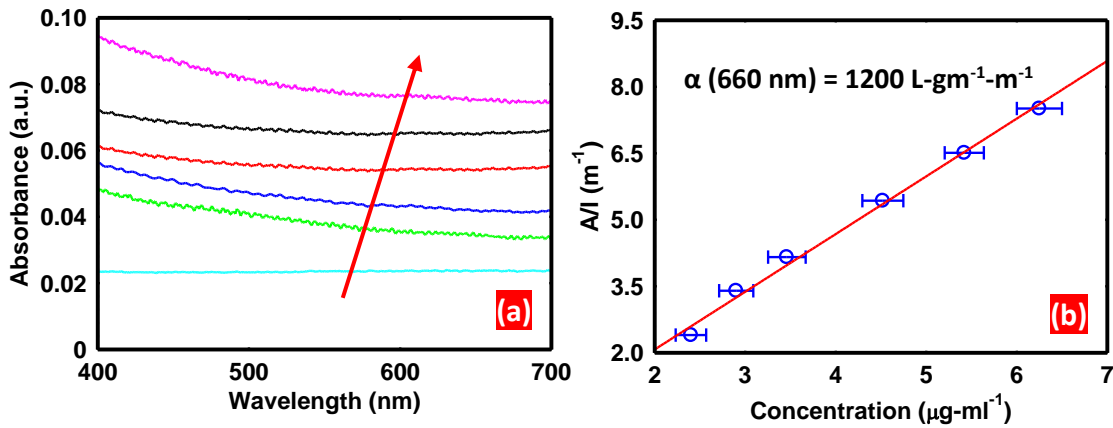


Figure S2: (a) Optical absorbance of graphene flakes dispersed in de-ionized water for different concentrations (from $2.4 \mu\text{g}\cdot\text{ml}^{-1}$ to $6.3 \mu\text{g}\cdot\text{ml}^{-1}$). Direction of arrow indicates the increasing order of concentration. Initial concentration, before centrifugation was $0.06 \text{ mg}\cdot\text{ml}^{-1}$. As expected, absorption spectra are featureless in visible region. (b) Optical absorbance (at $\lambda=660$ nm) divided by cell length (A/l) as a function of concentration for water/HOPG dispersion, showing Lambert-Beer behavior with molar absorptivity (α) of $1200 \text{ L-gm}^{-1} \text{m}^{-1}$. X-axis error bar denotes the uncertainty in measurement of the mass of graphene/graphite in aqueous solution.

S3.0 Correlation of AFM height profiles and Raman spectroscopic signatures of graphene layers:

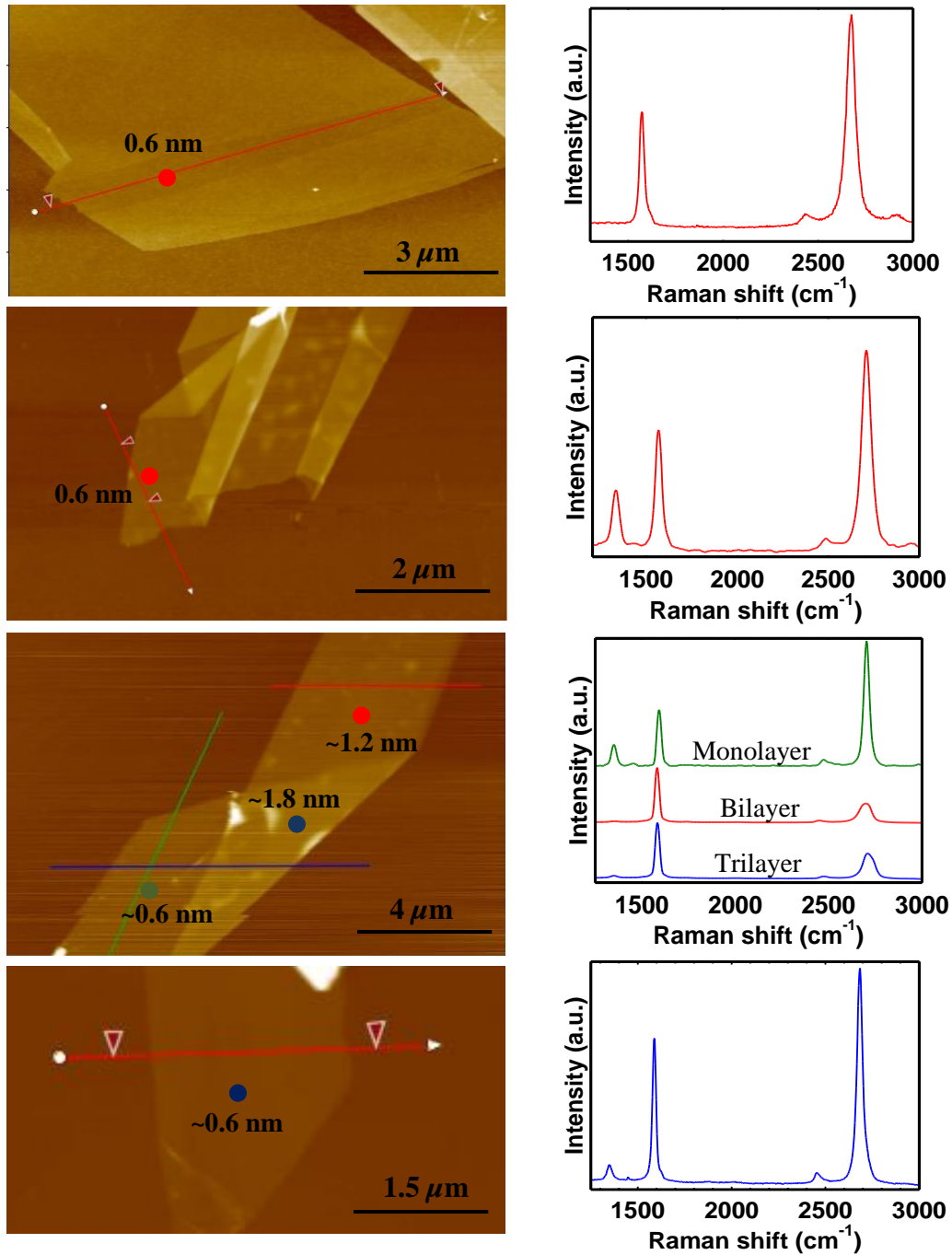


Figure S3: Correlation between layered thicknesses as observed by AFM and Raman spectroscopic signatures on a graphene flake. Raman signatures corresponding to monolayer graphene was observed at a flake thickness of ~ 0.6 nm whereas, Raman signatures corresponding to bilayer and trilayer graphene were observed at a flake thickness of ~ 1.2 nm and 1.8 nm, respectively. This correlation was done on several graphene samples mentioned in table SI.

S4.0 Graphene in water: Stability in a non-stabilizing medium:

As illustrated in Figure 1 (in manuscript), increase in sonication time from 7 hours to 12 hours, number fraction of monolayer graphene increases drastically (from ~5% to ~40%) whereas, number fraction of bilayer and trilayer decreases in proportion. It demonstrates that HOPG has been first exfoliated to relatively thick graphene layers and subsequently these thick layers were exfoliated to monolayer graphene even in water and exfoliation efficiency *i.e.* number fraction of graphene layers will depend on sonication process. However in a previous report⁵, it has been mentioned that water is not a good stabilizing solvent for graphene. For liquid phase exfoliation to occur, net energy cost (enthalpy of mixing per unit volume) should be very small. In this case, enthalpy of mixing can be expressed as⁴

$$\frac{\Delta H_{\text{mixing}}}{V_{\text{mixing}}} = \frac{2}{t} (\delta_{\text{Graphite}} - \delta_{\text{Solvent}})^2 \phi \quad (4)$$

where $\delta_i = (E_i)^{1/2}$ corresponds to square root of the surface energy (E_i) of the respective phase, t is the thickness of a graphene flake and ϕ is graphene volume fraction. From Eq. 4, it is clear that minimal energy will cost for exfoliation, if surface energy of the solvents matches with that of graphite. However, it is to be noted that water surface energy is ~100 mJ/m², which is away from the surface energy value reported for graphite and carbon nanotubes (40 – 90 mJ/m²). So it seems apparently that water is an unsuitable solvent for graphene dispersion and hence it cannot disperse/exfoliate graphene stably. This apparent contradiction between observed exfoliation in water (reported here) and thermodynamics described by Eq. 4 can be understood as follows: graphite or carbon nanotubes *if pristine*, exhibit surface energies as given above. However, it has been shown that surface energies are sensitive to structural modifications and can be efficiently altered with surface functionalization/doping in graphite or carbon nanotubes⁶⁻⁸. The specific type of substituted atoms or groups determines the specific surface potential *i.e.* surface energy. Moreover, it has been observed that increase in surface energy values could be observed upon mild oxidation of surface⁹. Figure S4 shows Raman spectra of pristine and functionalized HOPG. Before sonication, Raman D band is completely absent in thick HOPG flakes and evolves gradually during sonication process. In Figure 3, it has been illustrated that this D band is due to functionalization with solvent molecules (covalent attachment of oxygen and hydrogen). It

suggests that HOPG gets marginally functionalized during sonication process before exfoliation in to thin graphene layers. Functionalization causes increase in surface energy of HOPG and subsequently when surface energy of functionalized HOPG would be comparable to that of water, then in accordance with Eq. 4, exfoliation of HOPG in to thin graphene layers could be expected. This explains the observed high yield exfoliation of graphene layers in water medium in near equilibrium condition. Extent and effect of “*marginal functionalization*” on properties of exfoliated graphene layers are important aspect to be considered. We would like to emphasize that, the functionalization is marginal as evident from the Raman spectroscopic results and confocal Raman images of graphene monolayers exfoliated in water (see Figure 3 in manuscript and Fig. S17). It is clear that we get much superior quality Raman signatures as compared to those reported for graphene oxide^{9,10}. All these results summarize that although obtained graphene layers are functionalized but degree of functionalization is quite low to have severe effect on electronic properties of graphene layers (see section S10.0).

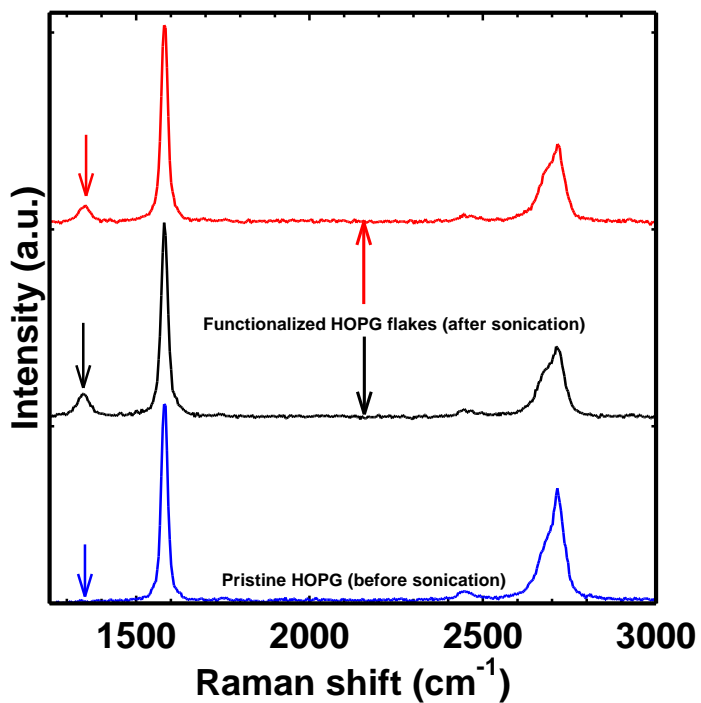


Figure S4: Raman spectra of pristine and functionalized HOPG flakes. Spectrum of pristine HOPG was acquired before sonication process whereas, for functionalized thick flake of HOPG, Raman spectrum was taken after transferring the flakes onto the SiO₂ substrates after 3-4 hours of sonication. Centrifugation was intentionally avoided in order to probe the functionalization effect on bulk HOPG flakes.

S5.0 AFM imaging of aged samples:

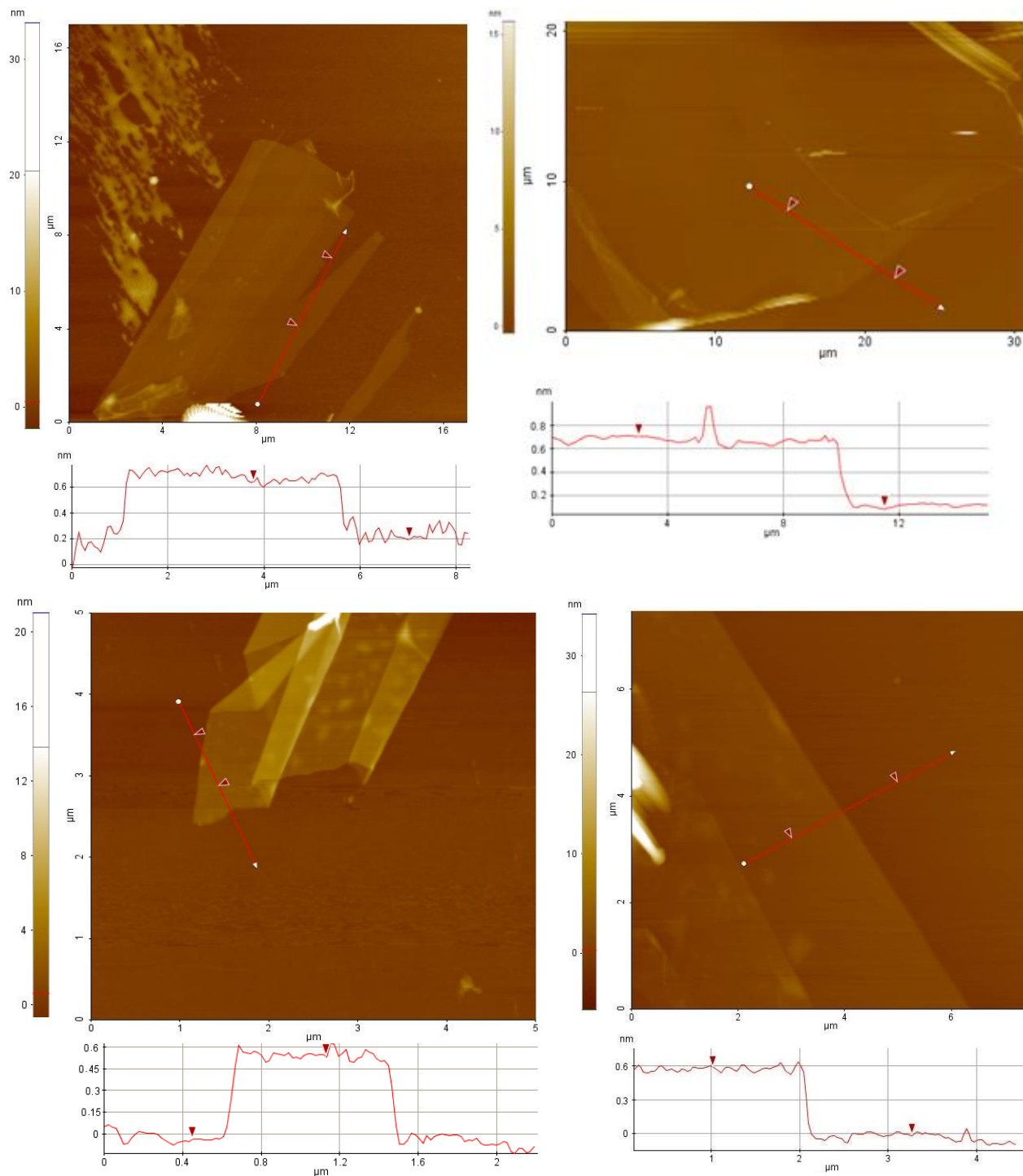


Figure S5: AFM micrograph of some of graphene flakes obtained from exfoliation of water/HOPG based dispersion immediately after centrifugation.

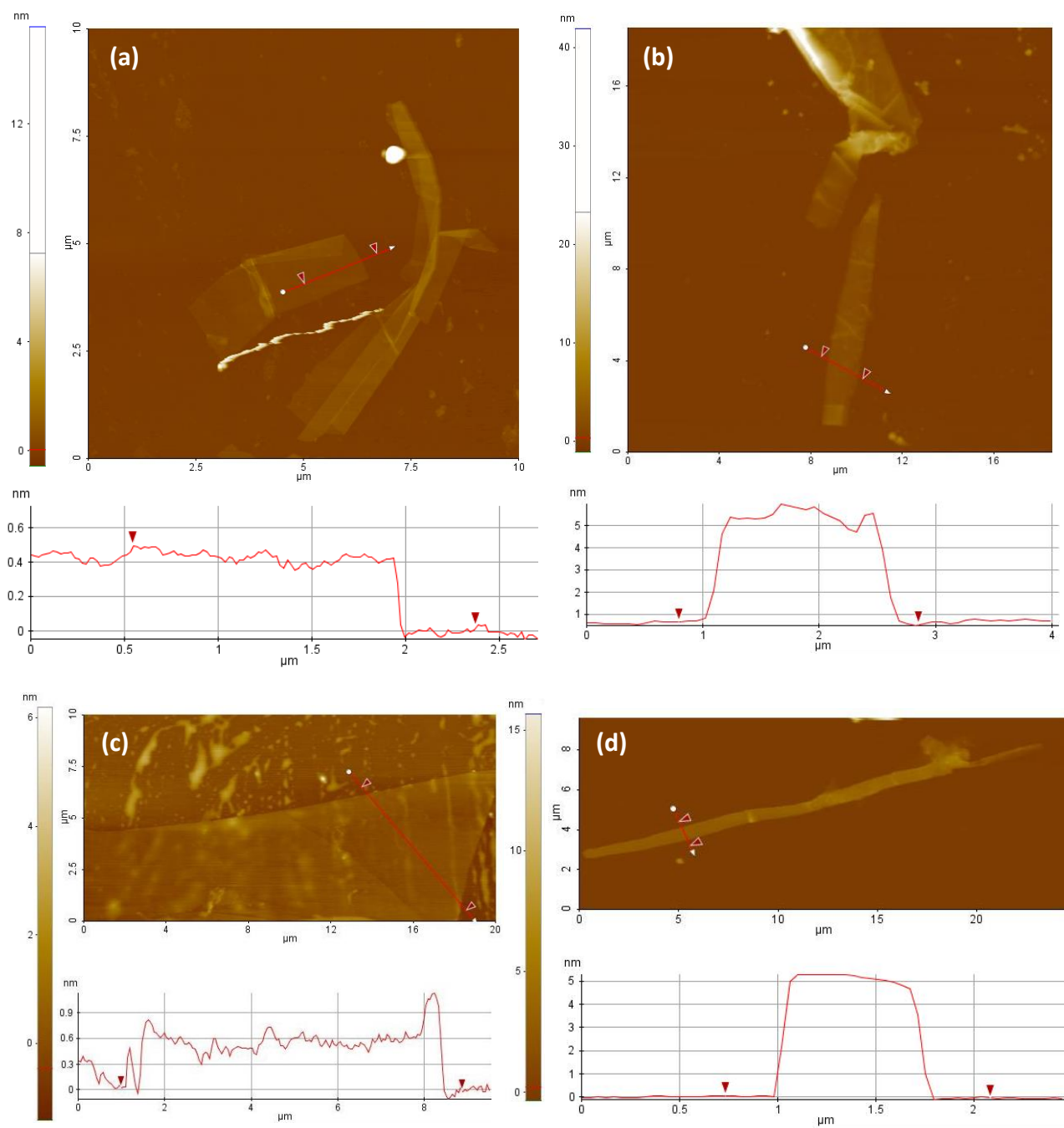


Figure S6: AFM micrograph of some of graphene flakes obtained from exfoliation of water/HOPG based dispersion after **(a, b)** 1 month and **(c, d)** 7 months of centrifugation.

S6.0 Dynamic light scattering experiment: Flake size determination of suspended graphene layers in dispersion:

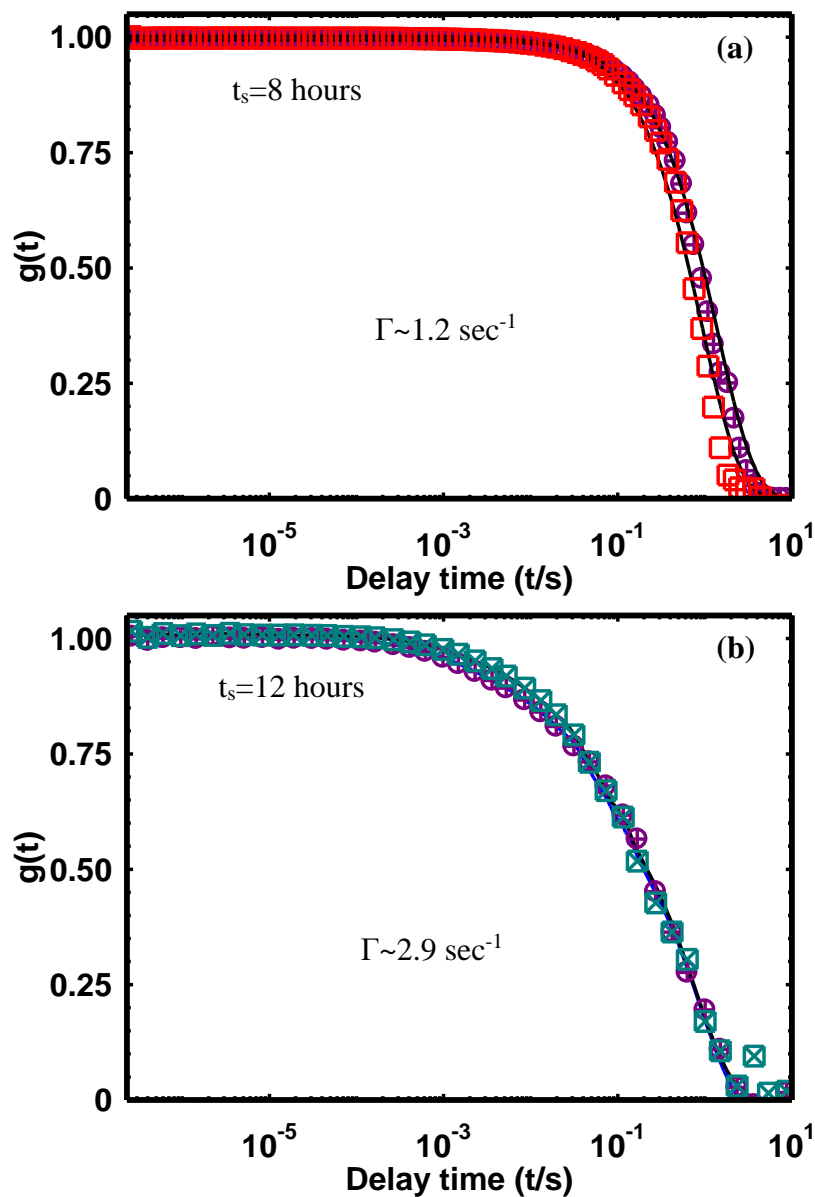


Figure S7: Dynamic light scattering experiment showing exponential decay of normalized dynamic correlation function, $g(t)$ with delay time for graphene dispersions sonicated for (a) 8 hours, (b) 12 hours. Centrifugation time was fixed for 2 hours. Symbols are the data points and solid lines are the fits using equation 4. Decay rate (Γ) obtained by fitting is also given. This was done after transferring the top portion of the centrifuged solution (which contains most of the thin graphene layers) to another cylindrical vial used for experiment. Concentration of the solutions after centrifugation was between $6 \mu\text{gm}\cdot\text{ml}^{-1}$ to $8 \mu\text{gm}\cdot\text{ml}^{-1}$.

Light scattering measurement was done on water/graphene dispersions and resulting spectra are shown in Figure S9. It is to be noted that these DLS spectra were acquired on 2 hour

centrifuged solution, which is supposed to contain predominantly thin graphene layers. Hence, the size estimated from DLS experiments corresponds to that for thin layers. Obtained spectra were fitted using equation-

$$g(t) = a * \exp(-\Gamma t) \quad (5)$$

where a, is a constant pre-factor and Γ is decay rate. Decay rate is related to diffusion coefficient (D) as-

$$D = \frac{\Gamma}{\xi^2} \quad (6)$$

where, ξ is wave vector and is given as

$$\xi = \frac{4\pi n}{\lambda} \sin\left(\frac{\theta}{2}\right) \quad (7)$$

where n is refractive index of the solvent (in this case water); λ , wavelength of light used (632 nm) and θ is scattering angle (in this case it is 90°).

Experiment was repeated more than 25 times. Figure S9 illustrates two representative spectra corresponding to each sonication time. By putting the fitting parameters, size of large suspended graphene flakes was calculated to be $\sim 30 \mu\text{m} - 60 \mu\text{m}$ and $\sim 4 \mu\text{m} - 20 \mu\text{m}$, for sonication time of 8 hours and 12 hours, respectively. However, it is only fair to say that DLS was not performed on a dispersion containing only monolayer but we suggest that $\sim 20 \mu\text{m}$ flakes size extracted from DLS for 12 hour sonicated solution, corresponds to thin (1-3) graphene layers (see Figure 1g in manuscript). It also provides credence to our observation on flake sizes imaged using AFM, SEM and TEM.

S7.0 Recycling of the sediment:

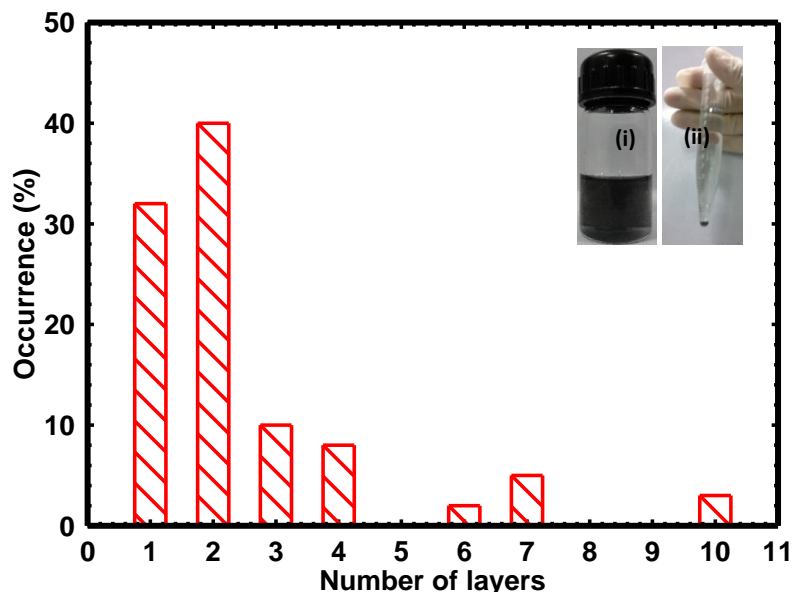


Figure S8: Histograms showing occurrence (number of visual observations) of graphene layers as a function of their respective layered structure, obtained after recycling process. Statistics shows that number fraction of ~30% could be achieved after recycling process which is very close to those obtained for fresh dispersion. Inset shows snapshots of sonicated and centrifuged solution after recycling process labeled as (i) and (ii), respectively.

We have observed that the remaining sediment after centrifugation can be efficiently recycled to get graphene layers without deteriorating their properties. Recycling was followed by drying the remaining sediment and then dispersion of dried sediment was prepared using de-ionized water. It gives the number fraction and mass fraction of ~32% (Figure S9) and 12.4 wt% respectively. Number and mass fractions for recycled dispersions were calculated exactly in the same way as calculated for fresh dispersions. These values are almost similar to those obtained from fresh water/HOPG dispersions suggesting the efficient recycling of sediments. Thus the actual yield of graphene monolayers will not be given by equation 2 as discussed above (2.45 wt%)

but will be described by $Y = \left(\frac{M_{mono}}{M_{all}} \right)$ with much higher yield of 16.6 wt% and 12.4 wt% for fresh and recycled dispersions, respectively. So, the efficient recycling of the sediments allows us to achieve high yield of monolayer graphene. Figure S11 shows the TEM images along with the diffraction patterns and Raman spectra of graphene layers after the recycling process suggesting that quality of the graphene layers remains unaffected after recycling process.

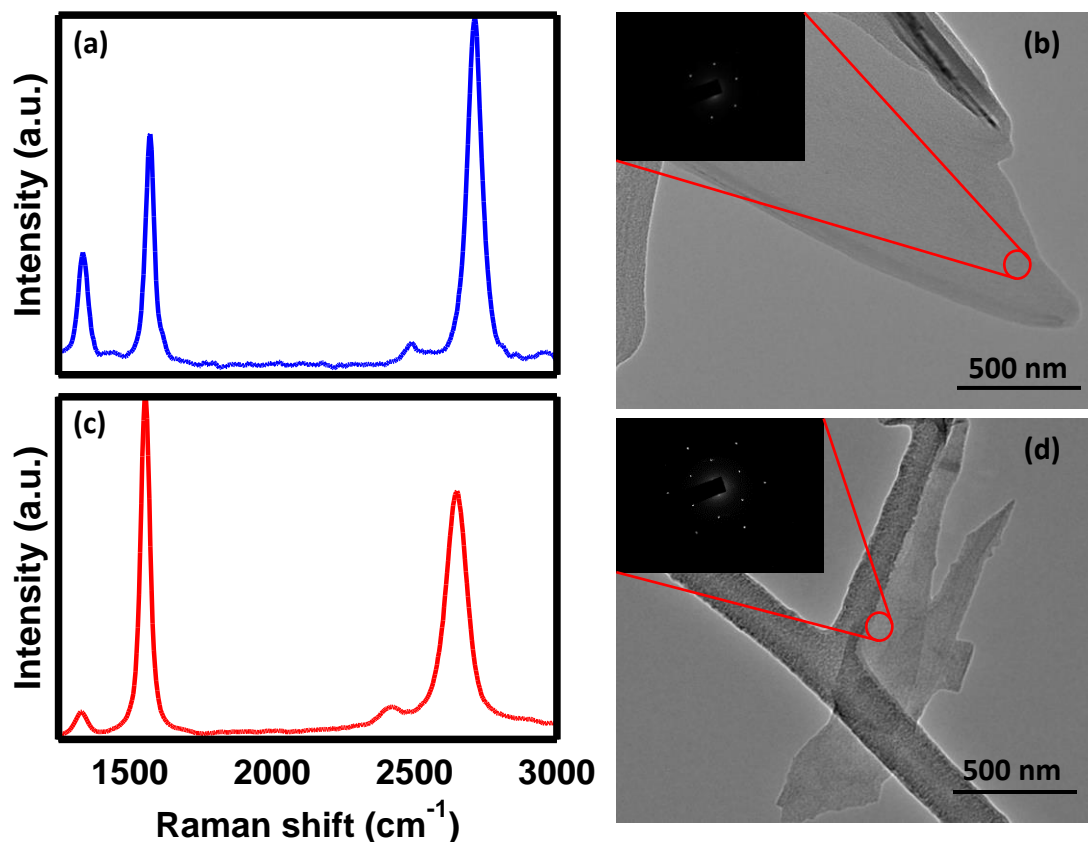


Figure S9: Raman spectra and TEM image along with electron diffraction of monolayer (a, b) and few layer graphene (c, d) synthesized after recycling of remaining sediment. Red circles show the approximate regions where electron diffraction patterns were acquired. Raman spectra and electron diffraction pattern resembles to those acquired for graphene layers obtained from fresh dispersions of water/HOPG.

	Total no. of flakes imaged	Number of monolayers	Size of graphene monolayers (μm)	Number of multi layers	No. fraction of Monolayer graphene (%)	Mass fraction of monolayer graphene (wt %)	Fraction of material (δ) remaining after centrifugation (%)	Overall yield (wt %)
g-water (fresh, $t = 0$)	50	20	10-15	30	40	16.6	14.6	2.45
g-water ($t = 1$ month)	40	4	7-10	36	10	5.4	14.6	0.80
g-water ($t = 7$ months)	40	2	7-10	38	5	1.3	14.6	0.22
g-water (recycled)	50	16	5	34	32	12.4	14.6	1.81

Table S1: Summary of the statistics generated by analyzing large no. of AFM images of graphene layers obtained using fresh ($t = 0$), one month old, seven months old and recycled water/HOPG dispersions. (Data corresponds to sonication time of 12 hours).

S8.0 AFM topographic images for graphene layers obtained by exfoliation of LDG in water:

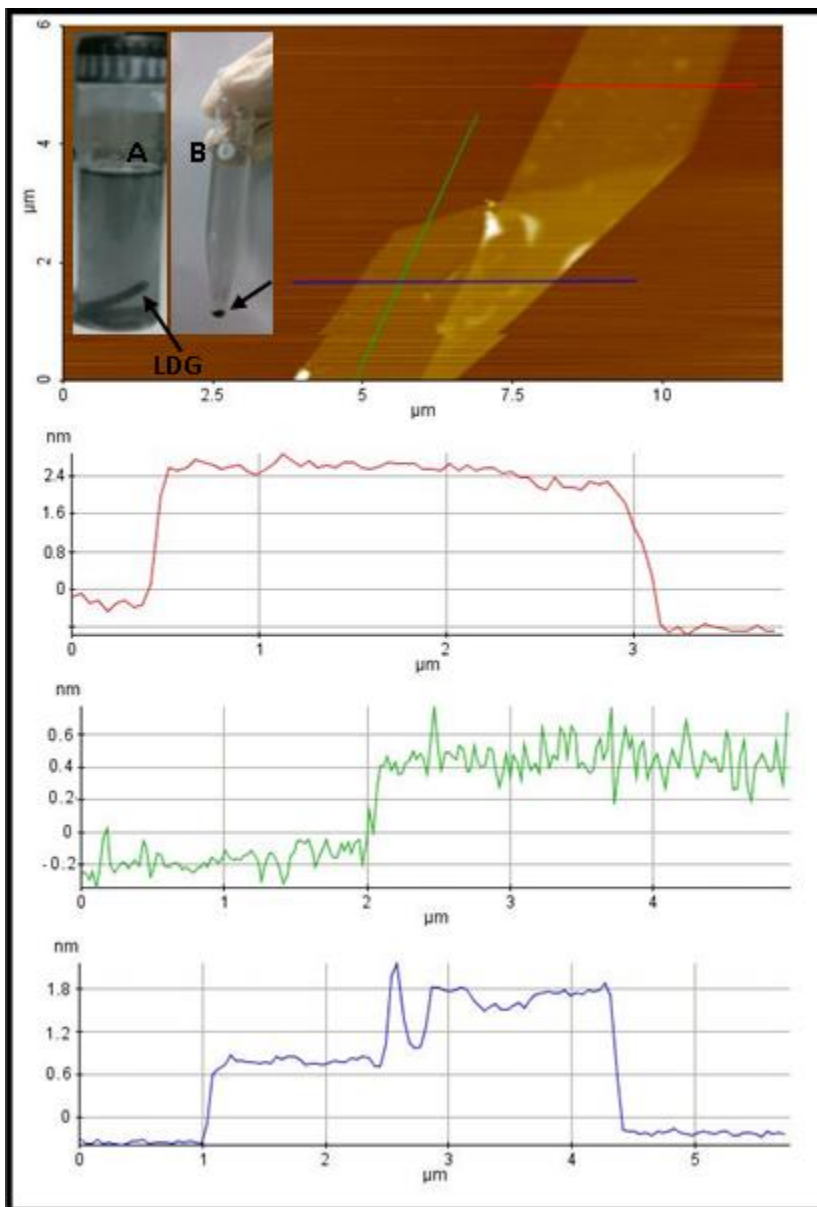


Figure S10: AFM topographic image and respective height profile of graphene layer obtained by exfoliation of LDG in water. Color of height profile resembles the colored lines in topographic image. Thickness of ~ 0.8 nm was obtained for monolayer graphene and thickness up to 2.5 nm was obtained for few layer graphene structures. Inset shows snapshots of sonicated and centrifuged solution labeled as A and B respectively. B shows fraction of sediment settled down after centrifugation as indicated by an arrow.

S9.0 Scanning electron micrograph of graphene samples prepared from exfoliation of LDG in water:

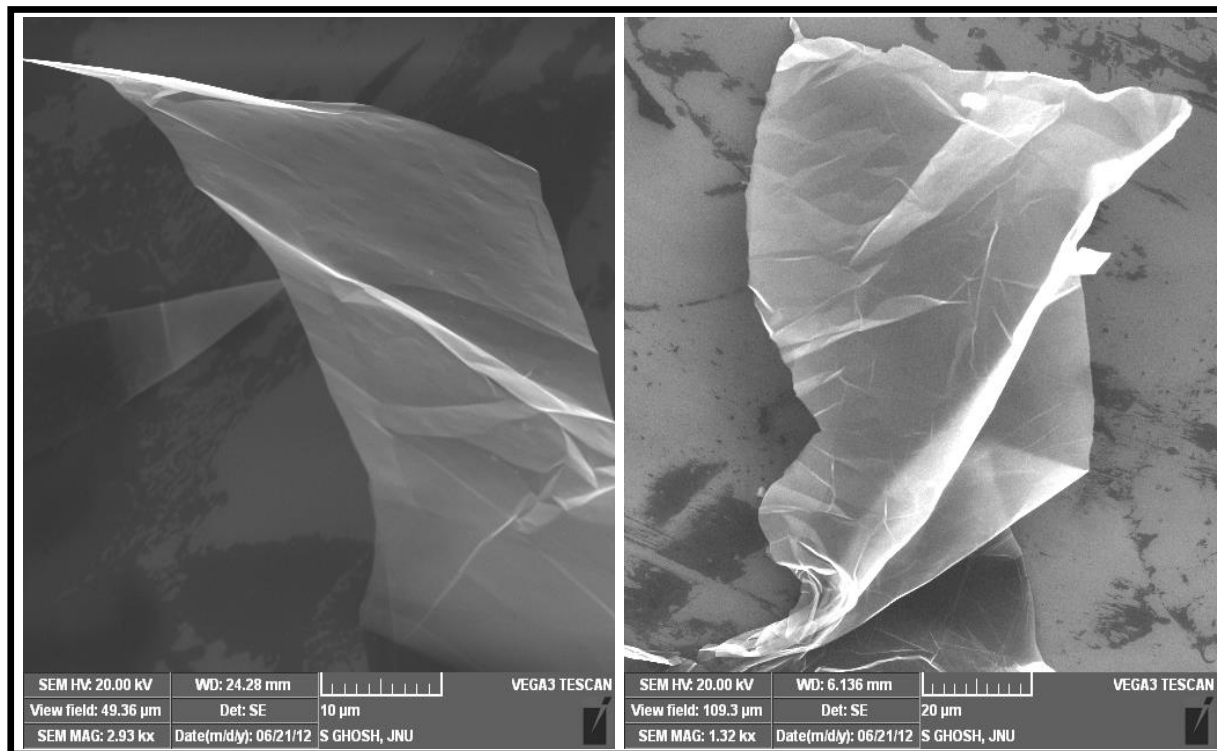


Figure S11: Scanning electron micrograph of few layer graphene obtained by exfoliated of low density graphite (LDG) in water. The size of graphene layers shown in figure varies from 50 to 80 μm.

S10.0 TEM image of graphene exfoliated in water (using LDG):

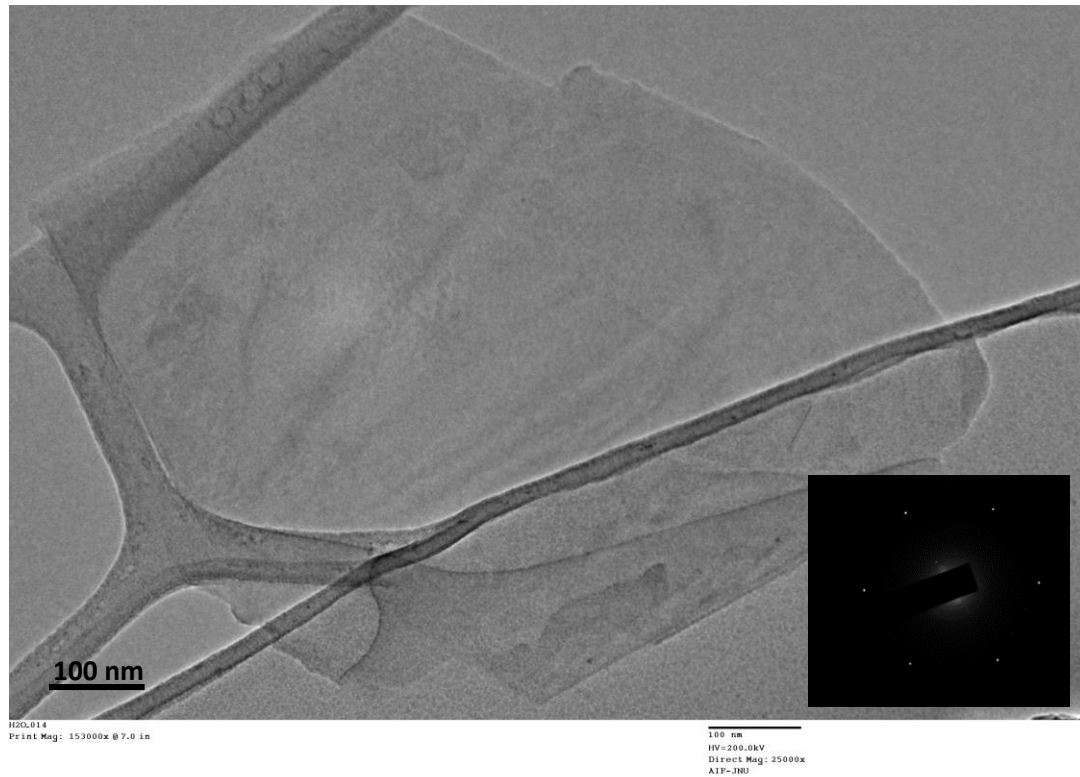


Figure S12: TEM image of graphene obtained by exfoliation of LDG in water. Bright spots arranged in a hexagonal geometry indicate that SAED pattern corresponds to monolayer graphene.

S11.0 TEM image of graphene exfoliated in water:

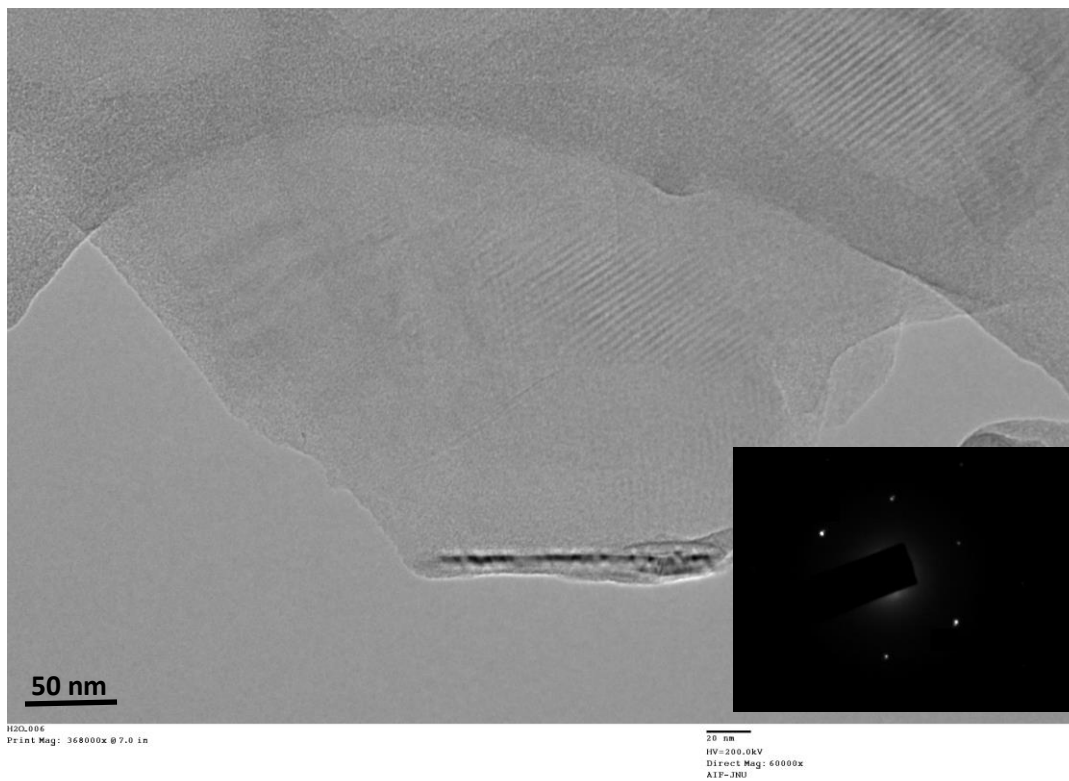


Figure S13: TEM image of graphene exfoliated in water. Corresponding SAED pattern is also given. SAED pattern consists of six bright spots with uniform intensity arranged in hexagonal symmetry for monolayer graphene.

S12.0 Lorentzian fitting of 2D peak of graphene - Identification of layered structure:

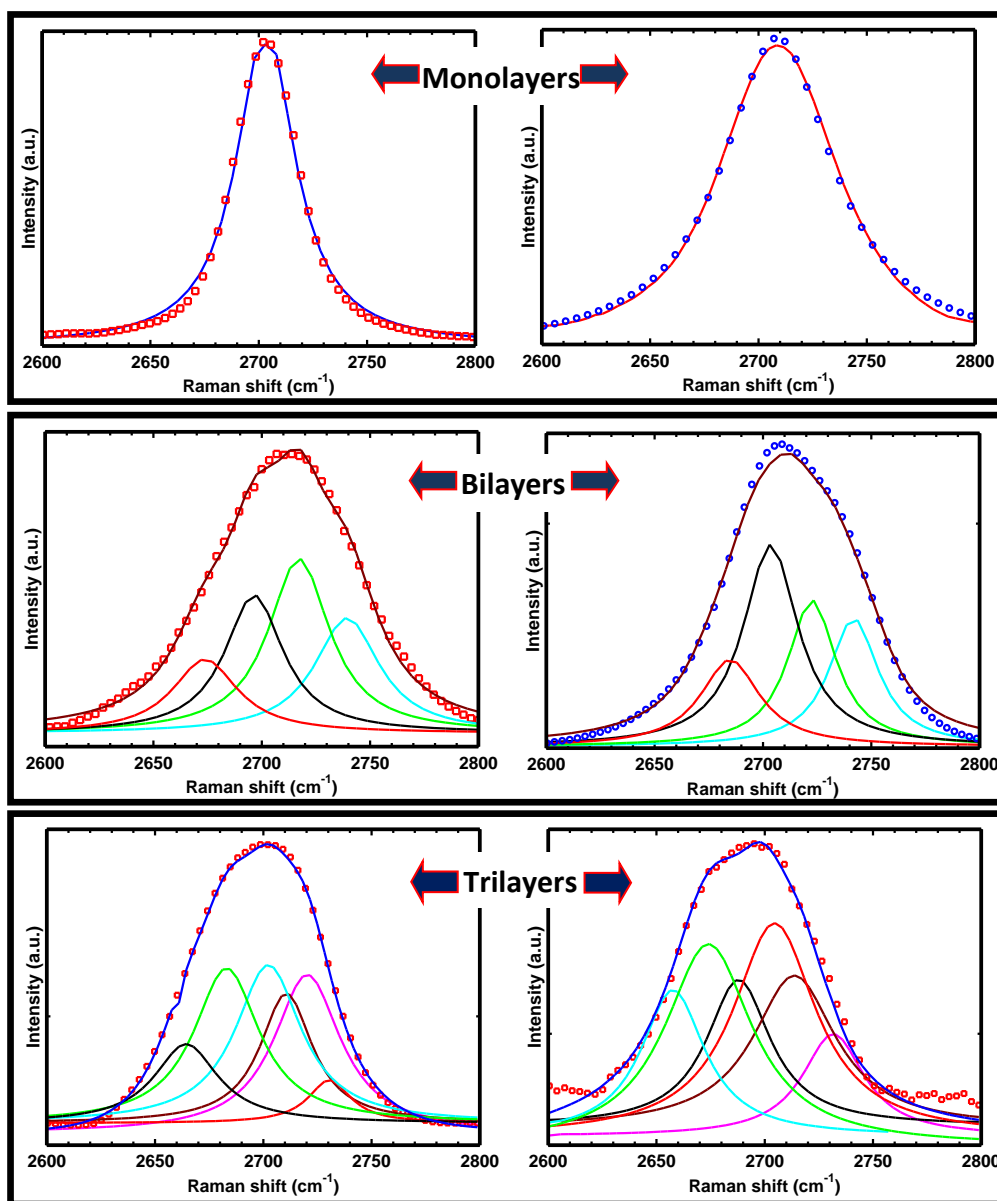


Figure S14: Lorentzian fitting of 2D peak of graphene monolayers and bilayers (left panel using HOPG and right panel using LDG). For monolayers 2D peak can be fitted with single sharp Lorentz peak whereas, 2D peak in bilayer splits into 4 peaks due to double resonance process or simply due to interaction between graphene planes. In exfoliation process, thickness of graphene layers can be controlled by adjusting sonication and centrifugation time. Existence of monolayer and bilayer graphene gives a clear hint that controllable growth of thin graphene layers is possible using this method.

S13.0 Confocal Raman mapping and spectroscopy for graphene exfoliated in water:

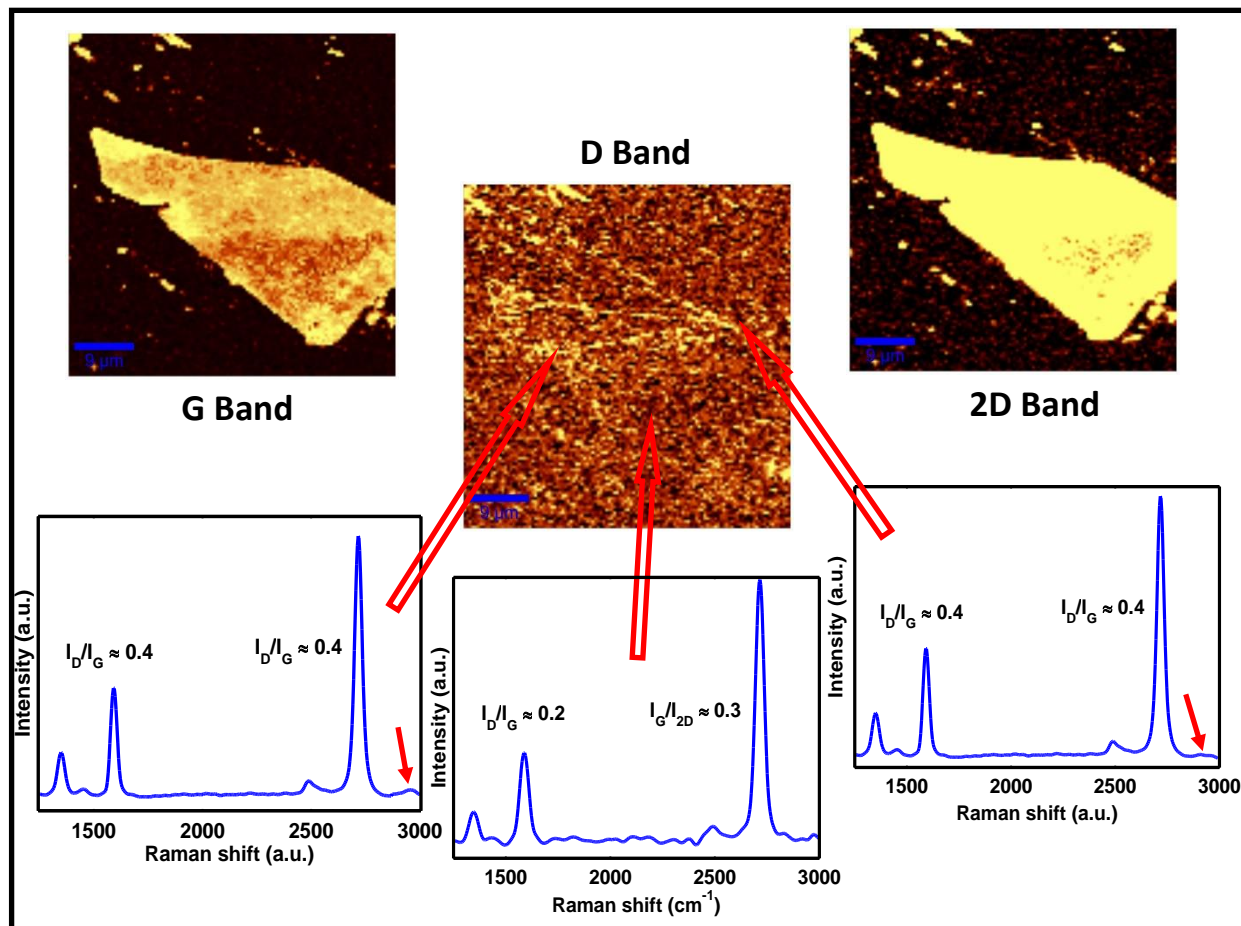


Figure S15: Confocal Raman mapping and spectroscopy of D, G and 2D peaks of Graphene exfoliated in water. Raman mapping of G and 2D peaks and intensity ratio (I_G/I_{2D}) at different portions of graphene flake (indicated by double red arrows) illustrates the uniformity of graphene layers. Raman peak corresponding to C-H stretching can be seen at ~ 2940 cm⁻¹ (indicated by single red arrows) Raman map of D peak and intensity ratio (I_D/I_G) illustrates that functionalization induced disorders are confined to edges of graphene flakes where $I_D/I_G \sim 0.4$ and are less effective at inner portion with $I_D/I_G \sim 0.2$ (marginally functionalized). Figure also shows that quality of graphene layer is better (lower I_G/I_{2D}) where defect density is minimum (lower I_D/I_G).

S14.0 Electronic structure calculations:

Density functional theory (DFT) was also used to understand the interaction of water molecule with the graphene sheets and to know the charge transfer between water molecule and graphene sheets in order to investigate the donor/acceptor character of water molecule onto the graphene surface. To find an energetically favorable structure and interaction strength between graphene and water molecules, DFT calculations were carried out using 3 different graphene models: (i) 19 rings (54 carbon atoms), (ii) 37 rings (96 carbon atoms), (iii) 61 rings (150 carbon atoms), where valences of edge carbon atom is satisfied with hydrogen (H) atom. Figure S18 shows the charge density map of combined entity *i.e.* water molecule adsorbed on graphene in the optimized geometry. It is clear from the front view of charge density maps that graphene surface is electron rich (red color), reflecting that charge were transferred from water molecule to graphene sheets. The amount of charge carrier transfer in terms of Mulliken charge is 0.379482e.

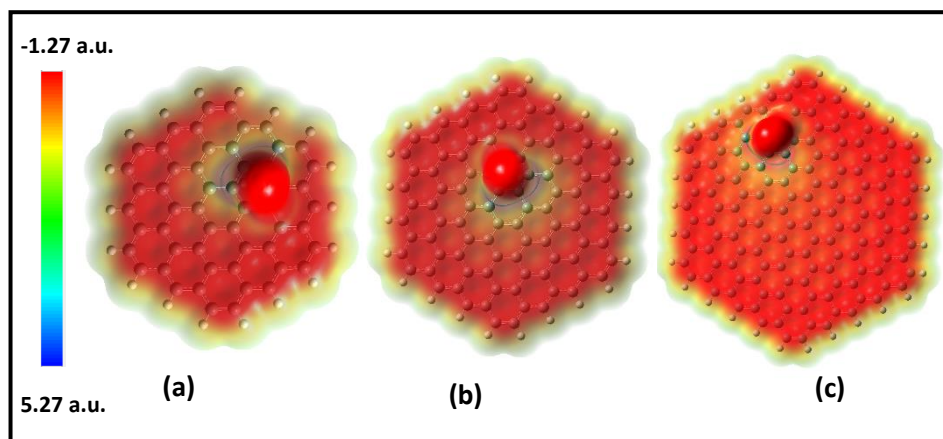


Figure S16: Front views of charge density map corresponding to energetically favorable structure of water molecule relaxed on graphene surface in the optimized configuration for (a) 19 rings, (b) 37 rings and (c) 61 rings respectively. Scale bar is given in terms of Mulliken charge which indicates the charge transfer from water molecules to polarizable graphene sheets resulting in *n*-type doping.

No. of H ions attached to graphene rings (96 carbon atoms)	No. of OH ions	Milliken charge (e) on graphene sheet
5	5	0.23634
5	4	0.02825
5	3	-0.23463
5	2	-0.38416
5	1	-0.66496

Table S2. Milliken charge transferred on graphene sheet (37rings or 96 carbon atoms) with fixed no. of H ions (5) and different no. of OH ions.

S14.1 Simulated infrared spectra

We would like to emphasize that around 100 cm^{-1} mismatch in the position of C-H vibrations (close to 2900 cm^{-1}) could be attributed to two possibilities

Finite size effect: It has been observed in simulated spectra that position of C-H vibrations shifts if we change the size of graphene rings (see Figure S17). Since, size of graphene rings in simulation and experiments are different, hence in view of finite size effect, $\sim 100\text{ cm}^{-1}$ of mismatch in the position of C-H vibration between simulated and experimentally observed IR spectra is plausible.

Environmental effect: In simulation, one H^+ ion is attached and one water molecule is adsorbed on to the graphene surface (in case of best possible trail structure). This case is different from the experimental circumstances where different number of H^+ ions and water molecules attached/adsorbed on graphene surface during exfoliation process could play an important role in deciding the vibrational frequencies of various functional groups. Moreover such contamination (adsorption of H^+ ions and water molecules) could also be introduced from ambient during IR measurement, resulting in such shift. Hence, effect of local environment could also be a factor responsible for this shift. A. Barth *et al.*¹⁹ have also observed such effect of the environment on vibrational frequencies while studying the infrared spectrum of proteins.

We would like to highlight that crucial point is the observation of vibrational signatures of similar functional groups in both simulation and experiments. However, mismatch between peak positions observed in simulation and experiments could be attributed to finite size and environmental effects as discussed above.

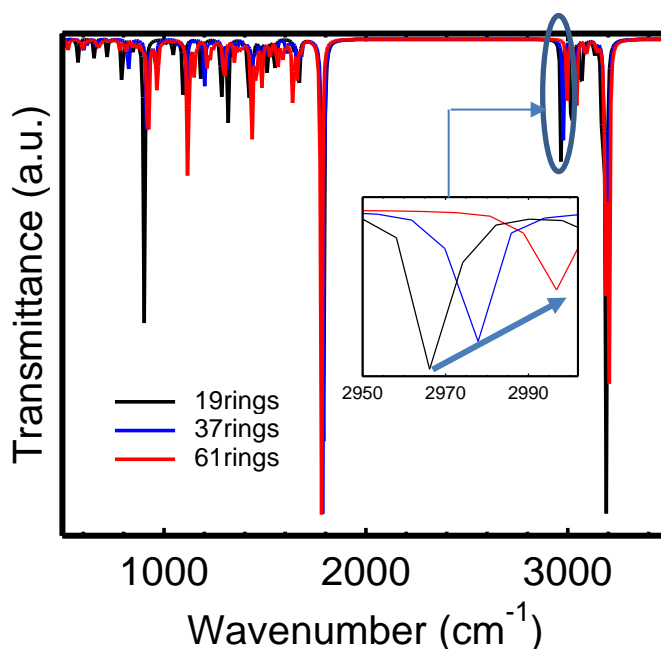


Figure S17. Simulated infrared spectra for different number of graphene rings in the best possible optimized geometry. Zoomed in graph corresponding to C-H vibrational frequency is also given in inset. It can be seen that C-H peaks shift to higher energy with increased number of graphene rings. This could be the possible reason behind a mismatch of 100 cm^{-1} in C-H vibrations in simulated and experimental IR spectra as given in Figure 4.

References:

1. A. C. Ferrari *et al.*, *Physical Review Letters* 2006, **97**, 187401.
2. J. C. Meyer *et al.*, *Nature* 2007, **446**, 60.
3. V. C. Tung, M. J. Allen, Y. Yang, R. B. *Nature Nanotechnology*, 2009, **4**, 25.
4. Y. Hernandez, *et al.* *Nature Nanotechnology*, 2008, **3**, 563.
5. C. J. Shih, *et al.* *JACS*, 2010, **132**, 14638.
6. M. H. Ghatee, *et al.*, *Journal of Chemical & Engineering Data* 2012, **57**, 2095.
7. R. Bose, *Journal of Physical Chemistry C* 2013, **117**, 20991.

8. S. C. Roh, *et al.*, *Polymer* 2014, **55**, 1527.
9. N. S. McIntyre, M. J. Walzak, "New UV/Ozone Treatment Improves Adhesiveness of Polymer Surfaces," *Modern Plast.*, 79-81, (March 1995).
10. D. Yand, *et al.* *Carbon* 2009, **47**, 145.
11. D. Li, M. B. Muller, S. Gilje, R. B. Kaner, G. G. Wallace, *Nature Nanotechnology*, 2008, **3**, 101.
12. X. Díez-Betriu, *et al.* *Journal of Materials Chemistry C* 2013, **1**, 6905.
13. A. C. Ferrari, *Solid State Comm.*, 2007, **143**, 47
14. A. C. Ferrari, D. M. Basco, *Nature Nanotechnology* 2013, **8**, 235.
15. C. M. Gee, *et al.* *Displays* 2013, **34**, 315–319.
16. L. Zhang, *et al.* *Carbon* 2009, **47**, 3365–3368.
17. Li. Zheng, *et al.* *J. Phys. Chem C* 2015, **119**, 5995.
18. P. H. Ho, *et al.* *ACS Nano* 2012, **6**, 6215.
19. A. Barth *Biochimica et Biophysica Acta (BBA) - Bioenergetics* 2007, **1767**, 1073.